

Three-dimensional passive sensing photon counting for object classification

Seokwon Yeom^{*a}, Bahram Javidi^b, and Edward Watson^c

^aSchool of Computer and Communication Engineering, Daegu University, Jillyang, Gyeongbuk, South Korea 712-714;

^bDept. of Electrical and Computer Engineering, U-2157, University of Connecticut, Storrs, CT USA 06269-2157;

^cU.S. Airforce Research Laboratories, Wright Patternson, Air Force Base, Dayton, OH USA 45433

ABSTRACT

In this keynote address, we address three-dimensional (3D) distortion-tolerant object recognition using photon-counting integral imaging (II). A photon-counting linear discriminant analysis (LDA) is discussed for classification of photon-limited images. We develop a compact distortion-tolerant recognition system based on the multiple-perspective imaging of II. Experimental and simulation results have shown that a low level of photons is sufficient to classify out-of-plane rotated objects.

Keywords: Automatic target recognition, Pattern recognition and feature extraction, Rotation-invariant pattern recognition, Three-dimensional image processing, Photon counting, Integral imaging, Passive sensing.

1. INTRODUCTION

Pattern recognition in scenes has been researched in military and industrial applications [1-4]. In integral imaging (II), three-dimensional (3D) information of rays is recorded using a micro-lenslet array [5-7]. Each micro-lenslet generates an elemental image with different perspective of objects. 3D scenes can be reconstructed optically or numerically in the opposite way of the recording. The object recognition and depth estimation using II have been researched in the literature [8-11]. For photon-counting imaging, there have been various applications such as night vision, laser radar imaging, radiological imaging, stellar imaging, and medical imaging [12-24]. Photon-counting imaging systems in general require less power than the conventional imaging systems that generate irradiance images.

In this keynote address, we present 3D distortion-tolerant classification using photon counting II [24]. The photon counting linear discriminant analysis (LDA) is discussed to classify out-of-plane rotated objects [24]. In the photon-counting LDA, we train the irradiance images of the objects and recognize the objects using the photon counts detected. The photon-counting LDA maximizes the Fisher's criterion in the Fisher's LDA [25,26] using photon-limited images. Euclidean distance between unknown input vector and the trained class-conditional mean vectors is adopted for decision making. The discrimination capability is evaluated by the correct and false classification rates as a function of varying number of photons. The experimental and simulation results show the photon-counting LDA can classify the distorted objects with a low level of photons.

The organization of this paper is as follows. In Section 2, we briefly review the advantages of II. The photon-counting LDA is discussed with the decision rule and performance metrics in Section 3. Experimental and simulation results are presented in Section 4. Conclusions follow in Section 5.

2. INTEGRAL IMAGING

In II sensing, we use a micro-lenslet array to record irradiance and directional information of rays from 3D objects. II reconstruction is the reverse of the recording process. We can perform optical and numerical reconstruction from

*yeom@daegu.ac.kr

elemental images. Multiple-perspective imaging is possible by a single shot to build a compact 3D recognition system. In this paper, photon-limited scenes are assumed to be generated by a photon-counting detector for the decision making. Photon-limited scenes with multiple perspectives are recorded according to the corresponding lenslet as shown in Fig. 1(a).

3. CLASSIFICATION OF PHOTON-LIMITED IMAGES

In this section, we discuss the photon counting LDA and the decision rule [24]. Let a column vector composed of the irradiance values of the pixels be one realization of a random vector $\mathbf{x} \in \mathbf{R}^{d \times 1}$, where $\mathbf{R}^{d \times 1}$ is d -dimensional Euclidean space, and d is the number of pixels in the scene. For photon-limited images, a random vector \mathbf{y} is composed of numbers of photons detected. Each component of \mathbf{y} follows independent Poisson distribution. In the experiments, the random vectors \mathbf{x} and \mathbf{y} , respectively are the irradiance and the photon event vectors corresponding to one elemental image. The following relationships hold for the first and the second moments between the irradiance random vector \mathbf{x} and the photon event random vector \mathbf{y} :

$$\boldsymbol{\mu}_y = N_p \boldsymbol{\mu}_x, \quad (1)$$

and

$$\Sigma_{yy} = N_p \text{diag}(\boldsymbol{\mu}_x) + N_p^2 \Sigma_{xx}, \quad (2)$$

where $\boldsymbol{\mu}_x$ and $\boldsymbol{\mu}_y$ are the mean vectors of \mathbf{x} and \mathbf{y} , respectively, Σ_{xx} and Σ_{yy} are the covariance matrices of \mathbf{x} and \mathbf{y} , respectively, and N_p is an expected number of photon-counts in the scene. The within-class covariance matrix and the between-class covariance matrixes of \mathbf{y} are, respectively derived as

$$\Sigma_{yy}^W = N_p \text{diag}(\boldsymbol{\mu}_x) + N_p^2 \Sigma_{xx}^W, \quad (3)$$

and

$$\Sigma_{yy}^B = N_p^2 \Sigma_{xx}^B, \quad (4)$$

where Σ_{xx}^W and Σ_{yy}^W are the within-class covariance matrices of \mathbf{x} and \mathbf{y} , respectively, and Σ_{xx}^B and Σ_{yy}^B are the between-class covariance matrices of \mathbf{x} and \mathbf{y} , respectively.

The photon counting LDA is defined as

$$\mathbf{z} = W_p^T \mathbf{y}, \quad (5)$$

where W_p maximizes the following criterion which is the same with the Fisher's LDA:

$$\begin{aligned} W_p &= \arg \max_{W \in \mathbf{R}^{d \times r}} \frac{|W^T \Sigma_{yy}^B W|}{|W^T \Sigma_{yy}^W W|} \\ &= \arg \max_{W \in \mathbf{R}^{d \times r}} \frac{|W^T \Sigma_{xx}^B W|}{|W^T [\text{diag}(\boldsymbol{\mu}_x) / N_p + \Sigma_{xx}^W] W|}. \end{aligned} \quad (6)$$

The column vectors of W_p are eigenvectors of $(\Sigma_{yy}^W)^{-1} \Sigma_{yy}^B$ corresponding to non-zero eigenvalues of $(\Sigma_{yy}^W)^{-1} \Sigma_{yy}^B$.

The rank of Σ_{yy}^B is the same with that of Σ_{xx}^B . The maximum value of $|W_p^T \Sigma_{yy}^B W_p| / |W_p^T \Sigma_{yy}^W W_p|$ is equal to the summation of non-zero eigenvalues of $\{W_p^T [\text{diag}(\boldsymbol{\mu}_x) / N_p + \Sigma_{xx}^W] W_p\}^{-1} \Sigma_{xx}^B$. It is noted that the photon counting LDA does not suffer from the singularity problem to obtain the inverse of Σ_{yy}^W . Therefore, the photon-counting LDA can handle a high dimensional images without any dimensional reduction process.

Euclidean distance between unknown input vector and the trained class-conditional mean vectors is chosen for the decision metric. In the experiments, the photon-limited integral image (a set of elemental images from one lenslet array) is obtained from different object orientations. During the test, the multiple photon event vectors are used to take advantage of the multiple perspective imaging, thus, the test vector for an unknown input scene is

$$\mathbf{z}_{test} = W_p^t \sum_{n=1}^{n_{test}} \mathbf{y}_{test}(n), \quad (7)$$

where $\mathbf{y}_{test}(n)$ is the photon event vector corresponding to the n -th photon-limited elemental image and n_{test} is the number of elemental images tested. We classify a vector \mathbf{z}_{test} as the member of class \hat{j} if

$$\hat{j} = \arg \min_{j=1, \dots, n_c} \|\mathbf{z}_{test} - \boldsymbol{\mu}_{z|w_j}\|, \quad (8)$$

where $\|\cdot\|$ stands for Euclidean norm, and $\boldsymbol{\mu}_{z|w_j}$ is the class-conditional mean vector. Assuming the distribution of \mathbf{y}_{test} is of the same as the distribution of the images \mathbf{y} used for training, we can show that

$$\begin{aligned} \boldsymbol{\mu}_{z|w_j} &= n_{test} W_p^t \boldsymbol{\mu}_{y|w_j} \\ &= n_{test} N_p W_p^t \boldsymbol{\mu}_{x|w_j}. \end{aligned} \quad (9)$$

Two performance measures are calculated: correct classification rate and false classification rate which are, respectively defined as

$$r_c(j) = \frac{\text{Number of decision for class } j}{\text{Number of test images in class } j}, \quad (10)$$

and

$$r_f(j) = \frac{\text{Number of decision for class } j, \text{ but are not in class } j}{\text{Number of test images in all classes except for class } j}. \quad (11)$$

4. EXPERIMENTAL AND SIMULATION RESULTS

The optical set-up is composed of a micro-lenslet array, an imaging lens, and a CCD camera. The focal length of each micro lenslet is about 3 mm, the focal length of the imaging lens is 50 mm, and the f -number of the imaging lens is 2.5. The imaging lens is placed between the lenslet array and the CCD camera due to the short focal length of the lenslets. Three classes of toy cars are used in the experiments as shown in Fig. 1(b). The size of three toy cars is about 2.5 cm \times 2.5 cm \times 4.5 cm. The distance between the CCD camera and the imaging lens is about 7.2 cm, and the distance between the micro-lenslet array and the imaging lens is about 2.9 cm. Integral images of the toy cars are gathered at rotation angles of 30°, 33°, 36°, 39°, 42°, and 45°. Rotation is with respect to the perpendicular to the optical axis of the micro-lenslet array. Thus, six integral images for each toy car are obtained; one at each of the six different out-of-plane rotation angles. Captured irradiance images are the same ones in [11] except that 30 (5 by 6) elemental images located in the center are used. The reference elemental image for the alignment is the central elemental image in the integral image of the object rotated at 36° for each class. After the alignment, each elemental image is cropped by 60 \times 125 pixels considering the computational load and accuracy of computing the linear discriminant function. Therefore, the dimension (d) of the vectors \mathbf{x} and \mathbf{y} is 7500 (=60 \times 125). The sizes of the integral image in the row and the column directions are 300 (=60 \times 5) and 750 (=125 \times 6), respectively. Figure 2 shows the integral images for toy cars with a rotation angle of 36°. For training, only one integral image is used for each class (object). That image is the one associated with a rotation angle of 36°. The other five integral images for each class are used only for testing. The integral image used for training in each class is composed of 30 elemental images, thus, the number of vectors (n_j) associated with training from each integral image is 30. The number of classes (n_c) is 3 so the total number of vectors (n) used in training process is 90 (=30 \times 3).

For the test, all of 18 integral images are used, including the three integral images used in training. Each integral image is considered an unknown input scene. 1000 photon-counting scenes are generated for each integral image and the correct and false classification rates are obtained from these 1000 realizations. The photon number is simulated by the Poisson random number generator in MATLAB with $N_p = 3$ for each elemental image normalized. The number of test elemental images, n_{test} is 30 since each integral image is composed of 30 elemental images. Therefore, the mean number of photon-counts ($N_p \times n_{test}$) in the entire scene (integral image) is 90 (=3 \times 30). The averaged classification results are illustrated in Fig. 3. The training and test are repeated with $N_p = 5$ and 10 when the corresponding mean numbers of photon-counts are 150 and 300, respectively. The averaged classification results are presented in Figs. 4 and 5, respectively. As illustrated in Figs. 3 to 5, a low level of photons can classify the distorted objects. The averaged correct classification rates increase when a larger number of photons are used while the averaged false classification rates decrease.

5. CONCLUSIONS

In this keynote address, a distortion-tolerant automatic recognition system using the photon-counting integral imaging is discussed. The photon-counting detector combined with the micro-lenslet array generates photon-limited multi-view scenes. Photon events are modeled by Poisson distribution. The photon-counting LDA is reviewed for the classification of photon-limited images. In the photon-counting LDA, the irradiance values are used for training while photon-limited images are tested to classify unknown input objects. A compact 3D information processing is possible and the performance can be enhanced by means of the multiple perspective photon-limited scenes of II.

REFERENCES

1. A. Mahalanobis and F. Goudail, "Methods for automatic target recognition by use of electro-optic sensors: introduction to the feature issue," *Appl. Opt.* 43, 207-209 (2004).
2. F. A. Sadjadi, ed., *Selected Papers on Automatic Target Recognition* (SPIE-CDROM, 1999).
3. H. Kwon and N. M. Nasrabadi, "Kernel RX-algorithm: a nonlinear anomaly detector for hyperspectral imagery," *IEEE Trans. Geosci. Remote Sens.* 43, 388-397 (2005).
4. B. Javidi, ed., *Optical Imaging Sensors and Systems for Homeland Security Applications* (Springer, New York, 2005).
5. J.-S. Jang and B. Javidi, "Time-multiplexed integral imaging for 3D sensing and display," *Optics and Photonics News* 15, 36-43 (2004).
6. F. Okano, H. Hoshino, J. Arai, and I. Yuyama, "Real-time pickup method for a three-dimensional image based on integral photography," *Appl. Opt.* 36, 1598-1603 (1997).
7. M. Martínez-Corral, B. Javidi, R. Martínez-Cuenca, and G. Saavedra, "Multifacet structure of observed reconstructed integral images," *J. Opt. Soc. Am. A.* 22, 597-603 (2005).
8. O. Matoba, E. Tajahuerce, and B. Javidi, "Real-time three-dimensional object recognition with multiple perspectives imaging," *Appl. Opt.* 40, 3318-3325 (2001).
9. Y. Frauel and B. Javidi, "Digital three-dimensional image correlation by use of computer-reconstructed integral imaging," *Appl. Opt.* 41, 5488-5496 (2002).
10. S. Kishk and B. Javidi, "Improved resolution 3D object sensing and recognition using time multiplexed computational integral imaging," *Opt. Express* 11, 3528-3541 (2003).
11. S. Yeom and B. Javidi, "Three-dimensional distortion tolerant object recognition using integral imaging," *Opt. Express* 12, 5795-5809 (2004).
12. J. W. Goodman, *Statistical Optics* (Jonh Wiley & Sons Inc., 1985), Chap 9.
13. G. M. Morris, "Scene matching using photon-limited images," *J. Opt. Soc. Am. A.* 1, 482-488 (1984).
14. E. A. Watson and G. M. Morris, "Comparison of infrared upconversion methods for photon-limited imaging," *J. Appl. Phys.* 67, 6075-6084 (1990).
15. E. A. Watson and G. M. Morris, "Imaging thermal objects with photon-counting detector," *Appl. Opt.* 31, 4751-4757 (1992).
16. M. N. Wernick and G. M. Morris, "Image classification at low light levels" *J. Opt. Soc. Am. A.* 3, 2179-2187 (1986).
17. L. A. Saaf and G. M. Morris, "Photon-limited image classification with a feedforward neural network," *Appl. Opt.* 34, 3963-3970 (1995).
18. D. Stucki, G. Ribordy, A. Stefanov, H. Zbinden, J. G. Rarity, and T. Wall, "Photon counting for quantum key distribution with Peltier cooled InGaAs/InP APDs," *J. Mod. Opt.* 48, 1967-1981 (2001).
19. P. A. Hiskett, G. S. Buller, A. Y. Loudon, J. M. Smith, I Gontijo, A. C. Walker, P. D. Townsend, and M. J. Robertson, "Performance and design of InGaAs/InP photodiodes for single-photon counting at 1.55 μm ," *Appl. Opt.* 39, 6818-6829 (2000).
20. L. Duraffourg, J.-M. Merolla, J.-P. Goedgebuer, N. Butterlin, and W. Rhods, "Photon counting in the 1540-nm wavelength region with a Germanium avalanche photodiode," *IEEE J. Quantum Electron.* 37, 75-79 (2001).

21. J. G. Rarity, T. E. Wall, K. D. Ridley, P. C. M. Owens, and P. R. Tapster, "Single-photon counting for the 1300-1600-nm range by use of Peltier-cooled and passively quenched InGaAs avalanche photodiodes," *Appl. Opt.* 39, 6746-6753 (2000).
22. P. Refregier, F. Goudail, and G. Delyon, "Photon noise effect on detection in coherent active images," *Opt. Lett.* 29, 162-164 (2004).
23. S. Yeom, B. Javidi, and E. Watson, "Photon counting passive 3D image sensing for automatic target recognition," *Opt. Express* 13, 9310-9330 (2005).
24. S. Yeom, B. Javidi, and E. Watson, "Three-dimensional distortion-tolerant object recognition using photon-counting integral imaging," *Optics Express*, Vol. 15, No. 4, pp 1513-1533 (February 19, 2007).
25. R. O. Duda, P. E. Hart, and D. G. Stork, *Pattern Classification 2nd ed.* (Wiley Interscience, New York, 2001).
26. K. Fukunaga, *Introduction to Statistical Pattern Recognition 2nd ed.* (Academic Press, Boston, 1990).

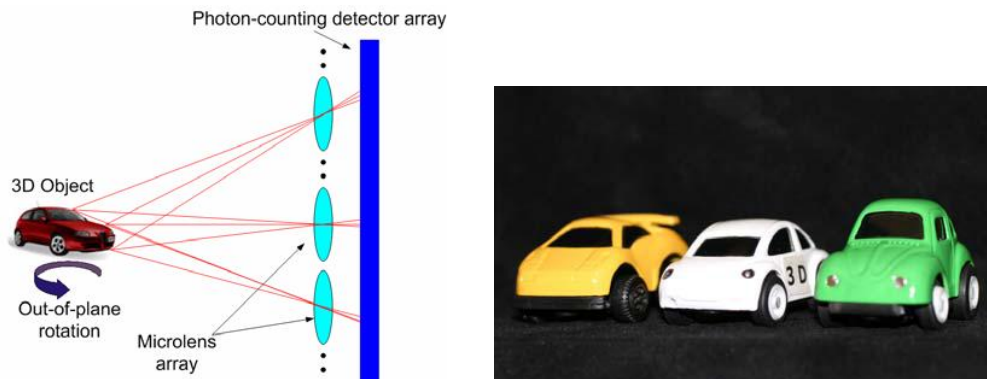


Fig. 1. (a) schematic diagram of photon counting integral imaging system, (b) three toy cars used in the experiments; car 1, 2 and 3 are shown from right to left.

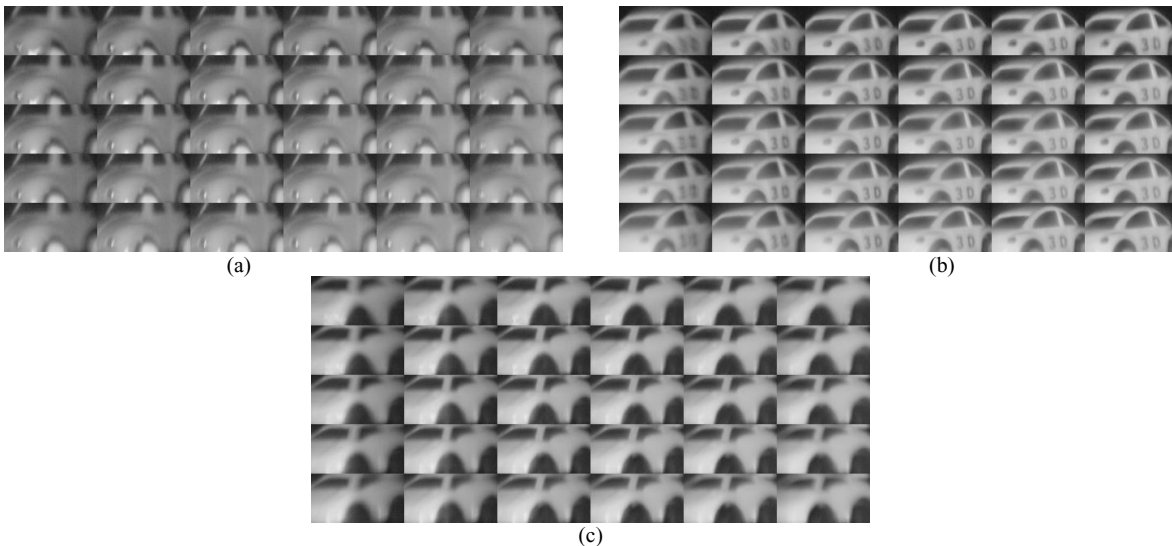


Fig. 2. Integral images of three objects associated with a rotation angle of 36° , (a) class 1, (b) class 2, (c) lass 3.

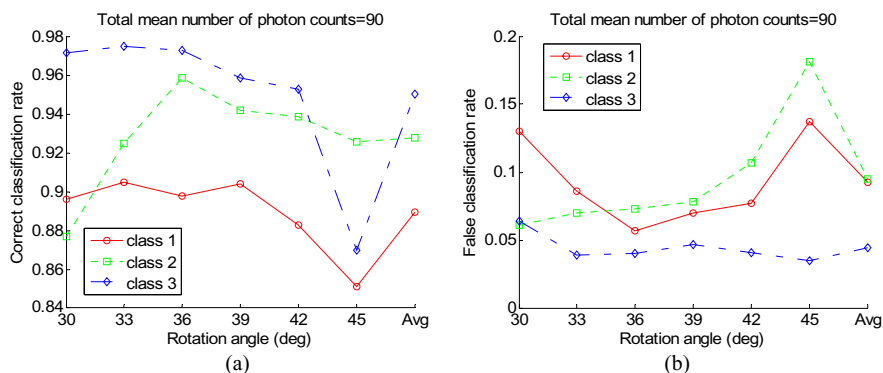


Fig. 3. Classification results when the mean photon number in the test scene is 90. (a) averaged correct classification rate for each class over 1000 runs, (b) averaged false classification rate for each class over 1000 runs. 'Avg' denotes the average value of 6 rotation angles.

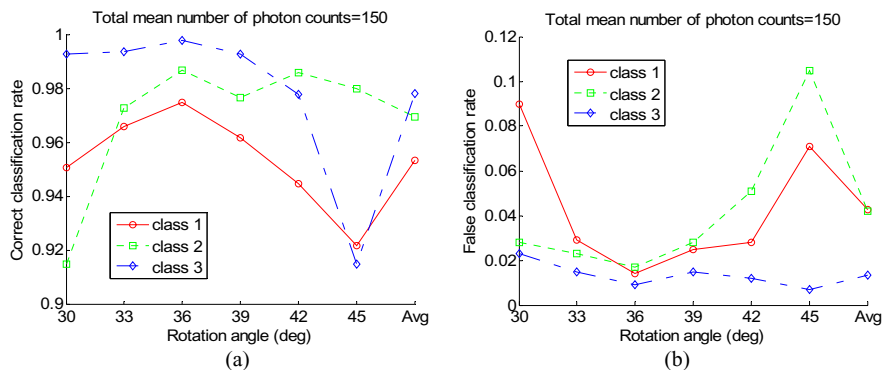


Fig. 4. Classification results when the mean photon number in the test scene is 150. (a) averaged correct classification rate for each class over 1000 runs, (b) averaged false classification rate for each class over 1000 runs. 'Avg' denotes the average value of 6 rotation angles.

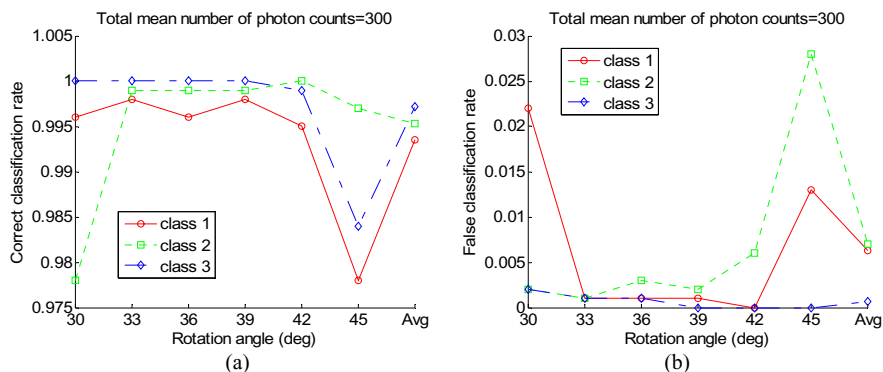


Fig. 5. Classification results when the mean photon number in the test scene is 300. (a) averaged correct classification rate for each class over 1000 runs, (b) averaged false classification rate for each class over 1000 runs. 'Avg' denotes the average value of 6 rotation angles.